Impact of Time-of-Flight Reconstructions on Maximum Standard Uptake Value in PET/MRI: Using of ^{18}F-FDG, ^{11}C-CFT and ^{11}C-PIB

Dewalage Dilani Neranjana Wimalarathne
Huazhong University of Science and Technology
Weiwei Ruan
Huazhong University of Science and Technology
Xun Sun
Huazhong University of Science and Technology
Fang Liu
Huazhong University of Science and Technology
Fan Hu
Huazhong University of Science and Technology
Xiaoli Lan (xiaoli_lan@hust.edu.cn)
Huazhong University of Science and Technology https://orcid.org/0000-0002-7263-7399

Original research

Keywords: Time-of-flight, PET/MRI, Quantification, SUVmax, Reconstruction

Posted Date: May 4th, 2021

DOI: https://doi.org/10.21203/rs.3.rs-439974/v1

Abstract

Objective: To evaluate the impact of time-of-flight (TOF) reconstruction on the maximum standard uptake value (SUV max) among ^{18}F-FDG, ^{11}C-CFT and ^{11}C-PIB in positron emission tomography/magnetic resonance imaging (PET/MR) brain images.

Methods: Suspected Alzheimer's and Parkinson's patients (AD/PD) who underwent ^{18}F-FDG, ^{11}C-CFT or ^{11}C-PIB PET-MR imaging were retrospectively included in the study. Each PET LIST mode data was reconstructed with and without TOF respectively using the system default three-dimensional ordered subset expectation maximization iterative reconstruction algorithm (3D-OESM). SUVmax of the selected brain volume of interest (VOI) were measured using the PMOD 3.906 PNEURO module in both TOF and non-TOF images. TOF and non-TOF SUVmax values were assessed by paired *t*-test and Pearson's correlation graphs. Contrast improvement of VOIs, relative % SUVmax difference and the percentage signal-to-noise ratio (%SNR) of whole-brain were measured using standard formulas.

Results: A total 109 patients were included with the median age (years) and body mass index (BMI-kg/m^2) of 62.2±6.8 y and 24.7±2.9 kg/m^2 in ^{11}C-PIB (n=34), 60.2±10.9 y and 23.9±3.7 kg/m^2 in ^{11}C-CFT (n=41) and 62.3±9.0 y, 23.6±3.5 kg/m^2 in ^{18}F-FDG (n=34), respectively. Higher average SUVmax values were observed in all the brain VOIs in TOF compared to non-TOF reconstructions, and relative % average SUVmax difference for all segmented brain VOIs were positive for all three radiotracers. Differences of SUVmax were significant in 100% of segmented VOIs in ^{18}F-FDG (P<0.01), similarly 83.34% of VOIs in ^{11}C-PIB (P<0.05), inversely not in ^{11}C-CFT. Contrast improvement was showed significant (P<0.05) for 60.0%, 66.7% and 50.0% of segmented VOIs in ^{18}F-FDG, ^{11}C-PIB and ^{11}C-CFT in TOF, respectively. %SNR gain for whole-brain showed slightly higher in ^{11}C-PIB and ^{18}F-FDG only in TOF, inequitably difference was significant (P<0.05) in ^{11}C-CFT non-TOF images. TOF versus non-TOF reconstructions were strongly correlated positively and differences were significant (P<0.01) in all the VOIs among three radiotracers.

Conclusion: The TOF reconstructions significantly improve the SUVmax value among all the brain VOIs in ^{11}C-PIB, ^{11}C-CFT and ^{18}F-FDG. Consequently, it enhanced image contrast and SNR. Thus, the quantitative effect of TOF reconstruction in simultaneous PET/MRI may positively impact the proper diagnosis of some diseases, such as Alzheimer's and Parkinson's diseases.

Introduction

Integrated positron emission tomography (PET) with magnetic resonance imaging (MRI) is clinically used to diagnose Alzheimer's (AD) and Parkinson's (PD) like neurodegenerative diseases in contemporary. The amalgamation of PET and MRI like two high-end technologies provide excellent anatomic information and functional MR imaging parameters with the metabolic and molecular information obtained from PET as a one-stop-shop for early and differential diagnosis of neurodegenerative diseases. PET tracers play a major role in diagnosing AD/PD, amongst ^{18}F-fluorodeoxyglucose (^{18}F-FDG) delivers early and sensitive

readouts of neural tissue loss, and more specific PET tracers now in use clinically, target dopaminergic deficiency (e.g. Dopamine transporter-^{11}C-CFT) or ß-amyloid plaques (e.g. Pittsburgh Compound B-^{11}C-PIB) in the brain.[1–6] Simultaneous acquisitions of MR imaging and PET data can be used to improve the accuracy of PET images and minimize the artefacts caused by motion due to different states of neuropathology and to reduce partial volume effects especially when imaging a small volume of interests (VOI).[7–10]

Another essential advantage of hybrid PET/MR in nuclear medicine is more accurate quantification values, i.e., standard uptake value (SUV). Quantification values from PET (some in the pico-molar range) of a large number of biological parameters are complemented by the high-resolution information provided by MRI (in the micro-molar range) to yield complementary information of previously unexpected variability in brain imaging.[9, 11] Subsequently SUVmax of metabolically active different key brain VOIs are potentially useful in diagnosing AD & PD if measurements are highly reproducible. Hence identifying which variables influence the measurements and to how much extent they may influence are key factors to consider in attempting to reduce the variability of the measurements.

The TOF (time-of-flight) technique is an important milestone in PET which initially demonstrated higher signal-to-noise (SNR) in reconstructed images compared with non-TOF mode, and later on, improved higher contrast recovery at a matched noise level in PET images. [12–14] The TOF system measures and records the time difference of two events and improves activity localization by more accurately identifying an annihilation event along a LOR (line of response).[15] Thus TOF results in a faster and more uniform convergence with 3D (three dimensional) iterative reconstruction, [13] similarly this possibly will also affect quantification in PET/MR imaging. An initial experimental phantom and clinical studies of TOF vs. non-TOF PET/MRI showed improved SNR, contrast recovery, image quality and quantitative accuracy and precision.[12–14]

Prior studies, revealed that SUVmax and distribution pattern of ^{18}F-FDG, ^{11}C-CFT and ^{11}C-PIB are vital measurements associated with different brain VOIs in prognosis, evaluation and treatment planning of AD/PD. [2, 16–22] Consequently, for ^{18}F-FDG, ^{11}C-CFT and ^{11}C-PIB PET/MR, the improvement in SNR and contrast recovery with TOF reconstruction possibly will be seen clinically as higher SUVmax in different brain regions in AD & PD, and this difference is expected to be greatest in smaller VOIs of the brain where the effect of contrast recovery is greatest. Significant in contrast recovery possibly will also be seen in larger patients due to the lower scatter fraction from adjusting soft tissues as seen with prior experimental phantom and clinical studies.[12–14] However, we assume ^{18}F-FDG, ^{11}C-CFT and ^{11}C-PIB radiotracers' biodistribution and uptake levels are rather different among various brain VOIs depending on the action of target radiopharmaceutical and pathology. On the other hand, Yang et al. and Dickson et al. pointed out that attenuation correction (AC) limits the quantitative accuracy of neurological PET/MR imaging. [23, 24]

According to our knowledge, there are some studies have been carried out to assess the reconstruction techniques versus quantification values and image quality parameters in TOF and non-TOF PET/MR

brain images [25, 26] However, there are no reported studies of evaluating TOF vs. non-TOF SUVmax in different brain VOIs among ^{18}F-FDG, ^{11}C-CFT and ^{11}C-PIB for diagnosing AD/PD. In a prospective setting, we assessed the impact of TOF technology in PET/MR imaging for diagnostic evaluation of the brain VOIs in AD/PD patients. Thus, the key purpose of this study was to determine if quantification differences are present in TOF compared to non-TOF among ^{18}F-FDG, ^{11}C-CFT and ^{11}C-PIB PET-MR imaging, then to conclude the quantitative magnitude of the differences are significant or not.

Methods

Ethical Statement

This retrospective experimental study of ^{18}F-FDG, ^{11}C-CFT and ^{11}C-PIB PET/MR in the diagnosis of AD and PD were performed at our institute, which has been approved by the Institutional Review Board of Union Hospital, Tongji Medical College, Huazhong University of Science and Technology. All the patients signed the informed consent.

Subjects

Patients suspected with Alzheimer's/Parkinson's diseases referred for ^{11}C-PIB, ^{11}C-CFT and ^{18}F-FDG PET-MR (n=109) studies were retrieved by an independent data analyst prior to automated SUVmax analysis by using the PNEURO module of PMOD 3.906 software.

PET/MR Imaging

All patients' acquisitions were performed on a SIGNA PET/MRI (GE Healthcare, Waukesha, USA) with subsequent specifications: 130 cm × 60 cm × 60 cm bore dimension, 3.0 Tesla superconductive magnet, gradient coils: 44 mT/m peak amplitude and 200 T/m/s peak slew rate, Detector type: SiPM, TOF, Cryogen Type: Liquid Helium. The mean injected radiation dose (MBq) and uptake time (minutes) for all three radiotracers are mentioned in **Table 1**.

All patients were asked to void before scanning begins. Prior to PET/MR, patients were given an instruction sheet and informed consent form to fill and to be submitted. Claustrophobic patients, patients with metal implants and uncooperative patients were excluded from the investigations. Placed the PETMR 8-channel Brain coil with mirror on the table on top of the adaptor. Patients were instructed verbally to keep the body align 90^0 degrees to the midsagittal plane on supine position, hands alongside the trunk and stay still 10, 15, 20 minutes for ^{11}C-CFT ^{18}F-FDG and ^{11}C-PIB, respectively. MR imaging of ^{11}C-PIB, ^{11}C-CFT and ^{18}F-FDG was performed with T1-weighted imaging (T1WI)-3D-BRAVO, three-dimensional gradient-echo sequence, flip angle = 12°, time of echo [TE]/time of repetition [TR] = 2.6/6.9 ms, bandwidth = 50 KHz, FOV = 24 cm × 24 cm, matrix = 384 ×384. PET was performed with 3D acquisition simultaneously. The images were reconstructed by using the three-dimensional ordered subset expectation maximum (3D OSEM) with 3-iterations, 28-subsets and a 3mm FWHM (Full Width of Half Maximum) Gaussian post-reconstruction filtering with filter. Default TOF (VUE FX) option was

applied for the TOF image group while VUE HD for the non-TOF image group. The attenuation correction was measured by atlas-based MRAC.

Image Analysis-Semi quantitative analysis

Reconstructed images were transferred from the scanner workstation to a data analysis PMOD Dell 32GB RAM/CORE i7+ workstation (PMOD version 3.906 Software, Zurich, Switzerland) for biomedical image quantification in different VOIs in the brain. PMOD-PNEURO Brain VOIs based on maximum probability atlas (Hammers-N30R83) [27] was used in segmenting brain regions. **Figure 1** gave an analysis example. T1 weighted images were employed for outlining anatomical structures. The selected VOIs of the brain for this study as follows, frontal lobe (FL), temporal lobe (TL), parietal lobe (PL), occipital lobe (OL), caudate nuclei (CN), nucleus accumbens (NA), putamen (PU), thalamus (TH), palladium (PA), substantia nigra (SN), anterior cingulate cortex (ACC), posterior cingulate cortex (PCC), cerebellum cortex (CC), brainstem (BS) and cerebellum medulla (CM). Statistics associated with standard uptake value, including maximum SUV (SUVmax), mean SUV (SUVmean), standard deviation SUV (SUVSD) and minimum SUV (SUVmin) of each VOI, were explored in all the ^{18}F-FDG, ^{11}C-CFT and ^{11}C-PIB brain images.

For the evaluation of image quality, two metrics have used the contrast of each brain VOI (***formula 01***), and signal-to-noise ratio (SNR) gain in the cerebellum VOI (***formula 02***) in different radiotracers. We calculated the contrast between the VOIs in the brain with reference to cerebellum cortex VOI. [28] The used radiotracers accumulate specifically in the cerebral cortex in AD/PD patients but those does not accumulate significantly in the cerebellum. Therefore, for obtaining contrast, VOI is set to the cerebellum cortical region.[29-31]

$$Contrast = \frac{SUV_{mean}(Segmented\ Brain_{VOI})}{SUV_{mean}(CC_{VOI})} \qquad (01)$$

The SNR of the whole-brain was calculated as a ratio of mean count difference of whole-brain (WB) VOI value to standard deviation (SD) of the same VOI according to the previous literature.[31]

$$SNR\ (WB_{VOI}) = \frac{SUV_{mean}(WB_{VOI}) - SUV_{mean}(CC_{VOI})}{SUV_{SD}(WB_{VOI})} \qquad (02)$$

Further, the differences in average SUVmax values are expressed as the relative percentage difference of non-TOF values (***formula 03***);

$$\%RAD - SUV_{max} = \frac{(SUV_{max}\ TOF - SUV_{max}\ nonTOF) * 100\%}{SUV_{max}\ nonTOF} \qquad (03)$$

Statistical Analysis

The IBM SPSS version 23.0 software was used to compare the TOF vs. non-TOF measurements. The comparisons among the SUVmax of different brain regions of TOF *vs.* non-TOF reconstruction methods, TOF-contrast *vs.* non-TOF-contrast, and TOF-SNR *vs.* non-TOF-SNR of whole-brain were analyzed using paired t-test. *P-value* < 0.05 was considered statistically significant level. The bivariate correlation analysis (Pearson's correlation) was used to see the relationship between TOF-SUVmax *vs*. non-TOF SUVmax in different brain regions. Significant correlation level measured as 0.01 (bilateral) Interpretation of Pearson's correlation coefficient performed according to previously published literature; a value ≤ 0.35 represent a weak correlation; a value between 0.36 and 0.67 represent a moderate correlation and a value between 0.68 and 1.0 represent a strong correlation, where a value of ≥ 0.9 represents a very strong correlation.[32] Bland-Altman plots were generated to show the clinical agreement between TOF and non-TOF reconstruction methods in whole-brain imaging among different tracers.[33]

Results

SUVmax

Overall higher average SUVmax values were observed in all the brain VOIs in TOF compared to non-TOF reconstructions in ^{11}C-CFT, ^{11}C-PIB and ^{18}F-FDG brain images (**Table 2**), though there was no statistically significant difference was observed with regards to the segmented VOIs of ^{11}C-CFT as depicted. Statistically significant differences (*P*<0.05) were seen in all the regions segmented for ^{11}C-PIB as shown in **Table 2** excluding Putamen and Cerebellum medulla. In ^{18}F-FDG, a statistically significant difference of *P*<0.01 were seen in all the brain regions.

Percentage of Relative average SUVmax difference - (% RAD-SUVmax)

The % RAD-SUVmax of segmented brain VOIs for the different three tracers were measured in TOF compared to non-TOF by ***formula 03***. The % RAD-SUVmax difference for all segmented brain VOIs were positive and % TOF SUVmax gains of ^{11}C-CFT, ^{11}C-PIB and ^{18}F-FDG are illustrated in **Figure 2.**

Image contrast

Image contrast of all brain VOIs was measured in TOF and non-TOF by ***formula 01***. Brain cortex regions (FL, TL, PL, OL, ACC and PCC) plus caudate nucleus, putamen and thalamus showed higher contrast in TOF compared to non-TOF in ^{18}F-FDG, further significant contrast (P<0.05) improvement was observed in all above regions in TOF. However, nucleus accumbens, palladium, substantia nigra, brainstem and cerebellar medulla showed higher contrast in non-TOF compared to TOF in ^{18}F-FDG, and significant

contrast (P<0.05) improvement was observed in palladium, substantia nigra and cerebellum medulla regions (**Figure 3A)**.

In ^{11}C-PIB **(Figure 3B)**, almost all the segmented brain VOIs showed higher contrast in TOF compared to non-TOF except the frontal lobe. Significant contrast improvement (*P*<0.05) was observed in key regions of the brain cortex, such as TL, PL, OL, ACC and PCC plus putamen, brainstem and cerebellum medulla. Caudate nucleus and Putamen VOIs showed higher contrast in TOF compared to non-TOF in ^{11}C-CFT **(Figure 3C)**. However, significant contrast improvement (P<0.05) was observed only in Putamen.

SNR in Whole-brain VOI

The % SNR gain measured in the whole brain was observed higher in ^{11}C-CFT and ^{11}C-PIB compared to ^{18}F-FDG. Though ^{11}C-PIB and ^{18}F-FDG show slightly higher % SNR in TOF brain images as illustrated in **Figure 3D** where ^{11}C-CFT found a higher % SNR gain in non-TOF brain images. However, a significant SNR enhancement (*P*<0.05) was seen only in ^{11}C-CFT in non-TOF images.

Correlation between the TOF and non-TOF SUVmax of different brain VOIs for the ^{11}C-CFT, ^{11}C-PIB and ^{18}F-FDG

The correlations of TOF *vs.* non-TOF were very high for all the VOIs of the brain for ^{11}C-CFT, ^{11}C-PIB and ^{18}F-FDG. It was observed strong positive correlation coefficients ($r^2 \geq 0.68$) and statistically significant difference (*P*<0.01) in TOF *vs.* non-TOF reconstructions of each segmented VOI for all the three radiopharmaceuticals (**Supplement Figure S1, S2 and S3)**.

Bland-Altman plot analysis for agreement of TOF and non-TOF method

The bland-altman analysis demonstrated that TOF and non-TOF reconstruction methods of whole brain are essentially equivalent as the average discrepancy (bias) was less significant and limits of agreements (LOA) were lie within narrow limits in ^{11}C-CFT (Bias-0.799≈0.8, L-LOA-1.541 to U-LOA 3.140) illustrated in **Figure 4A**,^{11}C-PIB (Bias-0.096≈0.1, L-LOA-0.254 to U-LOA 0.447) illustrated in **Figure 4B**, and ^{18}F-FDG (Bias-0.565≈0.57, L-LOA-1.208 to U-LOA 2.340) illustrated in **Figure 4C**, respectively. The difference between the two reconstruction methods was consistent with the increase of average SUVmax of both reconstructions in ^{11}C-CFT and ^{18}F-FDG. However, in ^{11}C-PIB it tends to deviate around the bias line after 2 g/ml of average SUVmax.

Discussion

This study evaluated the impact of TOF reconstruction on SUVmax values in several selected brain regions which remarks importance in diagnosing AD/PD among three radioactive tracers, ^{11}C-PIB, ^{11}C-CFT and ^{18}F-FDG, with hybrid PET/MR. It revealed that TOF reconstructions significantly affect on SUVmax values compared to non-TOF, and further improved the image contrast and % SNR. TOF and

non-TOF SUVmax shows a strong correlation in most of the brain VOIs for all three radiotracers. To the best of our knowledge, it is the first time that different tracers for brain quantification imaging were performed with TOF and non-TOF PET/MRI. The results suggested that TOF PET/MR brain imaging could be recommended for diagnosing AD/PD rather than using of non-TOF PET/MR modalities, however, multi-centre clinical trials should be carried out in future for further confirmation of our findings.

Although simulating phantom experiments [13] and initial patient studies with ^{18}F-FDG have been reported, [25] the quantitative effect would be different due to variances in radiotracer uptake and biodistribution within brain compartments, which also has benefitted in PET/MR for diagnosing neurodegenerative diseases by improving spatial resolution and SNR.[34] Early phantom studies demonstrated the improved contrast of the smallest spheres with TOF compared with non-TOF and confirmed the faster convergence of contrast with TOF. [12-14] These gains are evident from visual assessment of the images as well as a quantitative evaluation of contrast recovery of the spheres and noise in the background. The improvements with TOF are higher for larger objects.[35] Further above outcomes correlate with patient studies in which lesions (smaller VOIs) are seen more clearly and with higher uptake at comparable noise for TOF than with non-TOF.[13] Armstrong et al. explain the use of TOF and/or PSF (point spread function) reduced partial volume effects may increase lesion detectability. [36] Moreover TOF capable to minimize PET quantification bias substantially and significantly improve the quantitative accuracy of standard MRAC (Magnetic Resonance Attenuation correction) methods in PET/MR. [37]

Results showed significantly increased SUVmax of ^{18}F-FDG in TOF compared to conventional non-TOF reconstruction in all the brain VOIs. This is due to the higher uptake qualities of ^{18}F-FDG which can cause a higher scatter fraction in both TOF and non-TOF.[39] Further % RAD-SUVmax remains positively in all the brain VOIs. All the basal ganglionic regions (CN, PU, NA, PA and SN) showed higher % RAD-SUVmax in ^{18}F-FDG compared to PIB which indicated the normal higher uptake influence of ^{18}F-FDG in basal ganglionic regions. [17, 18] In cerebellar, cerebellar cortex showed slightly higher % RAD-SUVmax in ^{18}F-FDG (6.62%) compared to ^{11}C-PIB (5.26%). The commonly cerebellar cortex is considered as the reference region of normalizing the quantification values of these radiotracers in nuclear medicine in previous literature, due to its lack of affinity with this region and having homogeneity uptake appearance.[20, 29, 30]

Consequently, significantly increased SUVmax values were observed in all brain regions except the PU and CM in ^{11}C-PIB brain images in TOF compared to conventional non-TOF. Yet, CM is close to the significance level of $P<0.05$ which shown in **Table 2.** This result is due to low uptake patterns of ^{11}C-PIB in the putamen and cerebellar medulla regions, which cause relatively low scatter fraction contribution within the VOI, and could not benefit from improved quantitative accuracy using TOF technology. Increased % RAD-SUVmax in all brain cortex regions, (FL, TL, PL, OL, ACC and PCC) in ^{11}C-PIB compared to ^{18}F-FDG, this is due to the higher amyloid deposition in grey matter in cortex regions in AD patients.[38] Though cerebellar medulla showed a higher RAD-SUVmax % difference in ^{11}C-PIB (4.36%) compared to

^{18}F-FDG (4.03%), this result is caused due to non-specific ^{11}C-PIB retention in white matter and cerebrospinal fluid in CM [38].

In the ^{11}C-CFT brain, caudate nucleus and putamen regions were shown slightly higher SUVmax values in TOF compared to non-TOF, though there was no significance in results. **(Table 2)** Higher % RAD-SUVmax (10.7%**)** of ^{11}C-CFT in the caudate nucleus region was observed compared to ^{18}F-FDG (8.96%) and ^{11}C-PIB (8.47%), which may cause due to the higher uptake affinity of ^{11}C-CFT in the caudate nucleus.[40] However, in putamen it showed slightly lower RAD-SUVmax % in ^{11}C-CFT (7.74%) compared to ^{18}F-FDG (8.96%), this results may be due to the presence of PD positive patients within the suspected sample and it cause decrease uptake of ^{11}C-CFT in the putamen region which cause a low impact of TOF effect compared to ^{18}F-FDG.[41] However, the above-mentioned insignificance of several brain regions among different radiotracers' occurred due to lower uptake patterns and inefficient biodistribution were well explained in previous studies. [16, 17, 21, 22]

Previous studies of TOF PET/MR imaging has proved that TOF improves the contrast and signal to noise ratio. [35, 42] In this study, we measured the contrast of brain VOIs' SUV mean as a ratio with respect to the SUV mean of cerebellar cortex VOI as mentioned in ***formula 01*** in the method. Results proved that the TOF reconstructions significantly increased the average contrast of all brain cortex regions plus caudate nucleus, putamen and thalamus in ^{18}F-FDG. Though nucleus accumbens, palladium, substantia nigra, brainstem and cerebellar medulla did not show contrast enhancement in TOF compared to non-TOF in ^{18}F-FDG as shown in **Figure 3A.** This is due to the equal or higher uptake patterns in mentioned regions per the reference cerebellum cortex which cause not evident effect in TOF as we expected. In ^{11}C-PIB, significantly increased contrast was observed in all the brain VOIs with TOF except the frontal lobe, though the frontal lobe showed equal contrast gain in TOF and non-TOF. The outcome of the frontal lobe shows the similar uptake patterns do exist in the frontal lobe and cerebellar cortex. For ^{11}C-CFT, we observed higher contrast in both caudate nucleus and putamen regions, only putamen showed significance due to its high uptake properties of ^{11}C-CFT within, compared to caudate nuclei.

Figures of Pearson's correlation illustration shows TOF and non-TOF SUVmax measurements are strongly ($R^2 \geq 0.7$) positively correlated with significant difference among all the VOIs in the brain where reconstruction methods and SUVmax tends to increase together, which demonstrate TOF and non-TOF reconstructions equally impact towards the SUVmax value in the brain for ^{11}C-PIB, ^{11}C-CFT and ^{18}F-FDG. (**Figure S1-3)** Further, we performed the Bland-Altman analysis for these two reconstruction methods where it evaluates the clinical applicability of the both methods, it reveals that both reconstruction methods are fundamentally equal for the whole brain according to the results. (**Figure 4**)

One previous study revealed that new generation PET systems, which utilize new reconstruction method/s such as OSEM, PSF, and TOF could be misinterpreted the SUVs. [43] Though according to our study, TOF can enhance the SUVmax in several ways and make it closer to the actual SUVmax value, the quantitative accuracy of TOF and its impact in quantitative measurements such as SUV mean, SUVmax,

SUVSD and SUV peak of brain compartments in the assessment of brain pathologies should be investigated further in-depth.

Limitations of the study

Our study has several limitations. First, the smaller number of cases are included due to the retrospective study design, novelty of technology and time limitation for data collection of ^{11}C-PIB, ^{11}C-CFT and ^{18}F-FDG scans of suspected AD/PD patients which were archived in the PACS (Picture Archive and Communication System). A larger sample would possibly be needed to generalize these findings to a considerable population (e.g. a wider range of patient BMI (Kg/m2) and wider range of age). Second, for outlining most of cortical structures as the brain VOIs, PET-based MPA (Maximum Probability Atlas) was used due to avoid slowness or interruption of the segmentation process of the PNEURO module in PMOD 3.9 software, though T1 MR based parcellation is preferred to VOI outlining in deep nuclei and thalamus by PMOD team, thus the quality of the VOI definition in above-mentioned areas are reduced. For the effective use of PNEURO with high-resolution data, a high-end workstation (e.g. 8 core, 16GB or more RAM) is required. Third, our study did not address the clinical relevance of these quantitative measures, therefore a subsequent study with correlation of imaging parameters with patient diagnosis would be preferred. Fourth, the PET acquisition and reconstruction parameters used in our study were not optimized, required parameters such as iterations, subsets and FWHM selected for the reconstructions were the same used in our clinical setting. The same iteration was selected to reduce the noise generated by increasing iteration unnecessarily. Yet, these parameters concurrently provided a clinically detectable enhancement in contrast and SNR for SUVmax measurements in most regions of brain VOIs.

Conclusion

TOF reconstructions significantly improve the SUVmax value among several brain VOIs in ^{11}C-PIB, ^{11}C-CFT and ^{18}F-FDG images, and enhanced the contrast and SNR. We suggested that the quantitative effect from TOF reconstruction in simultaneous PET/MRI may positively impact the proper diagnosis of Alzheimer's and Parkinson's diseases.

Declarations

Ethics approval and consent to participate

This study is a retrospective study based on data from one of our clinical studies, in which all patients signed informed consent forms and the ethical approval was obtained by the Ethics Committee of Tongji Medical College, Huazhong University of Science and Technology.

Consent for publication

All authors have agreed to be so listed and have seen and approved the manuscript.

Availability of data and material

No other data and material.

Conflicts of interest

The authors declare that they have no conflict of interest.

Funding

This work was supported by the National Natural Science Foundation of China (No. 81701759 and 81901735)), the Key Project of Hubei Province Technical Innovation (2017ACA182), and the Clinical Research Physician Program of Tongji Medical College, Huazhong University of Science and Technology (No. 5001530008).

Authors' contributions

Wimalarathne DDN collected the data, performed the statistical analysis, and drafted the manuscript;

Ruan W, Sun X, Liu F and Hu F collected the data, and helped analysis the results;

Lan X contributed to the conception of the study, analysis the data, and revised the manuscript.

Acknowledgements

We thank for the team of PET tracer production in Department of Nuclear Medicine, Union Hospital, Tongji Medical College, Huazhong University of Science and Technology, for their work on different tracers.

References

1. Barthel H, et al. *PET/MR in dementia and other neurodegenerative diseases*. in *Seminars in nuclear medicine*. Elsevier; 2015.
2. Drzezga A. Diagnosis of Alzheimer's disease with [18F] PET in mild and asymptomatic stages. Behavioural neurology. 2009;21(1, 2):101–15.
3. Zhang XY, et al. PET/MR imaging: new frontier in Alzheimer's disease and other dementias. Front Mol Neurosci. 2017;10:343.
4. Yang ZL, Zhang LJ. PET/MRI of central nervous system: current status and future perspective. Eur Radiol. 2016;26(10):3534–41.
5. Drzezga A, et al., *Potential clinical applications of PET/MR imaging in neurodegenerative diseases*. Journal of Nuclear Medicine, 2014: p. jnumed. 113.129254.
6. Gao Z-B, et al. Multi-modality molecular imaging characteristics of dementia with Lewy bodies. J Int Med Res. 2018;46(6):2317–26.

7. Jadvar H, Colletti PM. Competitive advantage of PET/MRI. Eur J Radiol. 2014;83(1):84–94.
8. Littooij AS, et al. Potential clinical applications of PET/magnetic resonance imaging. PET clinics. 2013;8(3):367–84.
9. Torigian DA, et al. PET/MR imaging: technical aspects and potential clinical applications. Radiology. 2013;267(1):26–44.
10. Catana C, et al. PET/MRI for neurologic applications. Journal of nuclear medicine. 2012;53(12):1916–25.
11. Heiss W-D. The potential of PET/MR for brain imaging. Eur J Nucl Med Mol Imaging. 2009;36(1):105–12.
12. Surti S, et al. Investigation of time-of-flight benefit for fully 3-DPET. IEEE Trans Med Imaging. 2006;25(5):529–38.
13. Karp JS, et al. Benefit of time-of-flight in PET: experimental and clinical results. J Nucl Med. 2008;49(3):462–70.
14. Surti S. Update on time-of-flight PET imaging. J Nucl Med. 2015;56(1):98–105.
15. Lewellen T. Time-of-flight PET. Semin Nucl Med. 1998;28:268–75.
16. Navalpotro-Gomez I, et al. Nigrostriatal dopamine transporter availability, and its metabolic and clinical correlates in Parkinson's disease patients with impulse control disorders. Eur J Nucl Med Mol Imaging. 2019;46(10):2065–76.
17. Kalbe E, et al. Frontal FDG-PET activity correlates with cognitive outcome after STN-DBS in Parkinson disease. Neurology. 2009;72(1):42–9.
18. Nagasawa H, et al. PET study of cerebral glucose metabolism and fluorodopa uptake in patients with corticobasal degeneration. Journal of the neurological sciences. 1996;139(2):210–7.
19. Okello A, et al. Conversion of amyloid positive and negative MCI to AD over 3 years: an 11C-PIB PET study. Neurology. 2009;73(10):754–60.
20. Sun X, et al. Quantitative research of 11C-CFT and 18F-FDG PET in Parkinson's disease: a pilot study with NeuroQ software. Front NeuroSci. 2019;13:299.
21. Noh Y, et al. The role of cerebrovascular disease in amyloid deposition. J Alzheimers Dis. 2016;54(3):1015–26.
22. Silverman DH, et al. Positron emission tomography in evaluation of dementia: regional brain metabolism and long-term outcome. Jama. 2001;286(17):2120–7.
23. Dickson JC, O'Meara C, Barnes A. A comparison of CT-and MR-based attenuation correction in neurological PET. Eur J Nucl Med Mol Imaging. 2014;41(6):1176–89.
24. Yang ZL, Zhang LJ. PET/MRI of central nervous system: current status and future perspective. European radiology. 2016;26(10):3534–41.
25. Nagaki A, Onoguchi M, Matsutomo N. Clinical validation of high-resolution image reconstruction algorithms in brain 18F-FDG-PET: effect of incorporating Gaussian filter, point spread function, and time-of-flight. Nucl Med Commun. 2014;35(12):1224–32.

26. Shao X, et al. Applications of both time of flight and point spread function in brain PET image reconstruction. Nucl Med Commun. 2016;37(4):422–7.
27. Hammers A, et al. Three-dimensional maximum probability atlas of the human brain, with particular reference to the temporal lobe. Hum Brain Mapp. 2003;19(4):224–47.
28. Le Meunier L, et al. Enhanced definition PET for cardiac imaging. Journal of Nuclear Cardiology. 2010;17(3):414–26.
29. Tada T, et al. Comparative examination of the cerebellum and pons as reference regions for quantitative evaluation in PET imaging for Alzheimer's disease using11C-Pittsburgh Compound-B. J Nucl Med. 2019;60(supplement 1):3012–2.
30. Marcus C, Mena E, Subramaniam RM. Brain PET in the diagnosis of Alzheimer's disease. Clinical nuclear medicine. 2014;39(10):e413.
31. Lois C, et al. An assessment of the impact of incorporating time-of-flight information into clinical PET/CT imaging. J Nucl Med. 2010;51(2):237–45.
32. Taylor R. Interpretation of the correlation coefficient: a basic review. Journal of diagnostic medical sonography. 1990;6(1):35–9.
33. Doğan N. Bland-Altman analysis: A paradigm to understand correlation and agreement. Turkish Journal of Emergency Medicine. 2018;18(4):139–41.
34. Lindstrom E, et al. Brain-PET image reconstruction methods affect software-aided diagnosis in patients with neurodegenerative diseases. J Nucl Med. 2018;59(supplement 1):1780–0.
35. Akamatsu G, et al. Benefits of point-spread function and time of flight for PET/CT image quality in relation to the body mass index and injected dose. Clinical nuclear medicine. 2013;38(6):407–12.
36. Armstrong IS, et al. Impact of point spread function modelling and time of flight on FDG uptake measurements in lung lesions using alternative filtering strategies. EJNMMI physics. 2014;1(1):99.
37. Mehranian A, Zaidi H. Impact of time-of-flight PET on quantification errors in MR imaging–based attenuation correction. J Nucl Med. 2015;56(4):635–41.
38. Jack CR Jr, et al. 11C PiB and structural MRI provide complementary information in imaging of Alzheimer's disease and amnestic mild cognitive impairment. Brain. 2008;131(3):665–80.
39. Kimdon JA, Qi J, Moses WW. *Effect of random and scatter fractions in variance reduction using time-of-flight information*. in 2003 *IEEE Nuclear Science Symposium. Conference Record (IEEE Cat. No. 03CH37515)*. 2003. IEEE.
40. Heiss W-D, Herholz K. Brain receptor imaging. J Nucl Med. 2006;47(2):302–12.
41. Ishiwata K, et al. Development of PET radiopharmaceuticals and their clinical applications at the Positron Medical Center. Geriatr Gerontol Int. 2010;10:S180–96.
42. Akamatsu G, et al. Influences of point-spread function and time-of-flight reconstructions on standardized uptake value of lymph node metastases in FDG-PET. Eur J Radiol. 2014;83(1):226–30.
43. Prieto E, et al. Impact of time-of-flight and point-spread-function in SUV quantification for oncological PET. Clinical nuclear medicine. 2013;38(2):103–9.

Tables

Table 1 The patient information and the different tracer used

	^{11}C-CFT	^{11}C-PIB	^{18}F-FDG
Patients included (n)	41	34	34
Age (y)	60.2±10.9	62.2±6.8	62.3±9.0
BMI (kg/m^2)	23.9±3.7	24.7±2.9	23.6±3.5
Injection Dose (MBq)	3.9±1.4	4.3±1.1	3.8±0.6
Mean uptake time (min)	54.4±15.9	43.8±19.5	46.4±14.8

Table 2 Average SUVmax values in ^{11}C-CFT, ^{11}C-PIB and ^{18}F-FDG (mean ± SD)

	^{11}C-CFT			^{11}C-PIB			^{18}F-FDG		
Brain region	**TOF**	**non-TOF**	**p**	**TOF-**	**non-TOF**	**p**	**TOF**	**non-TOF**	**p**
Caudate Nuclei	8.34±2.31	7.53±2.16	0.122	1.29±0.39	1.19±0.34	0.000*	10.54±2.46	9.68±2.14	0.000*
Putamen	8.34±2.28	7.74±2.13	0.262	1.41±0.39	1.37±0.4	0.110	12.35±2.79	11.38±2.52	0.000*
Frontal Lobe	-	-	-	1.28±0.34	1.19±0.32	0.000*	10.45±1.88	9.97±1.77	0.000*
Temporal Lobe	-	-	-	1.20±0.3	1.11±0.28	0.000*	8.92±1.84	8.38±1.67	0.000*
Parietal Lobe	-	-	-	1.52±0.38	1.42±0.37	0.000*	12.33±2.75	11.69±2.51	0.000*
Occipital Lobe	-	-	-	1.39±0.36	1.32±0.36	0.001*	13.20±2.95	12.76±2.71	0.002*
Anterior cingulate cortex	-	-	-	1.39±0.38	1.27±0.36	0.000*	10.52±2.11	9.86±1.9	0.000*
Posterior cingulate cortex	-	-	-	1.46±0.46	1.34±0.41	0.000*	12.36±2.97	11.48±2.67	0.000*
Cerebellum Cortex	-	-	-	1.44±0.33	1.37±0.37	0.032*	10.96±2.49	10.28±2.22	0.000*
Brainstem	-	-	-	1.67±0.43	1.57±0.46	0.000*	10.11±2.16	9.29±1.94	0.000*
Cerebellum Medulla	-	-	-	1.63±0.38	1.56±0.41	0.054	10.02±2.59	9.63±2.52	0.007*
Thalamus	-	-	-	1.57±0.41	1.49±0.42	0.000*	11.80±2.58	11.19±2.46	0.000*
Nucleus Accumbens	-	-	-	-	-	-	8.96±1.85	8.68±1.75	0.000*
Palladium	-	-	-	-	-	-	9.95±2.15	9.45±2.04	0.000*
Substantia Nigra	-	-	-	-	-	-	7.56±1.72	7.336±1.58	0.003*

Figures

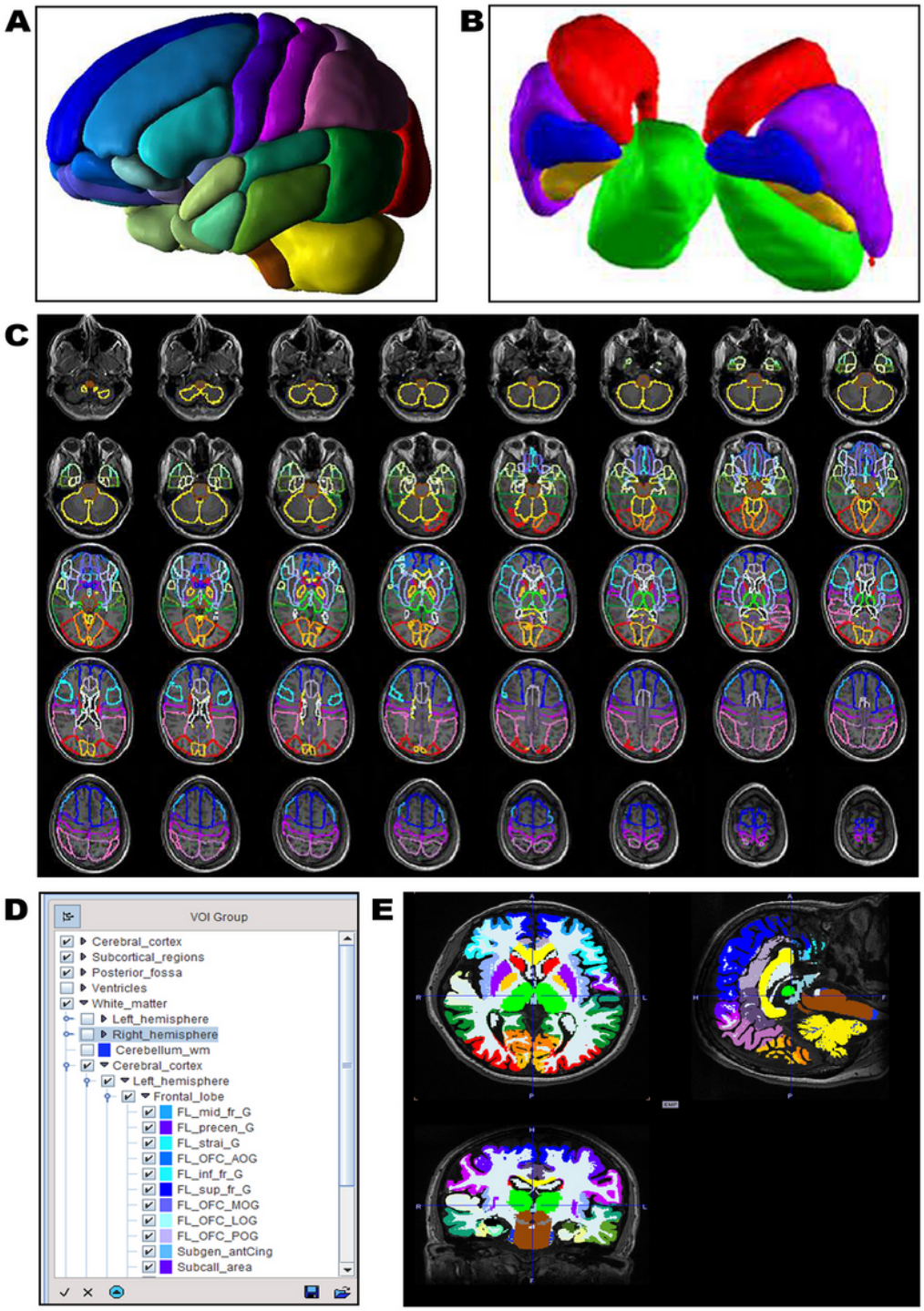

Figure 1

Reconstructed images analyses. A: The illustration shows a smoothed 3D surface rendering the 83 brain structures of the N30R83 atlas. It is clearly notable that the contours are not restricted to the gray matter pixels. B: The deep nuclei N30R83 structures are illustrated C: The figure illustrates the structures adjusted to a patient MRI. Only every third image slice is shown. D: Example for VOI selection E: Shows a layout of brain for the calculation of brain VOIs using the N30R83 Maximum Probability Atlas.

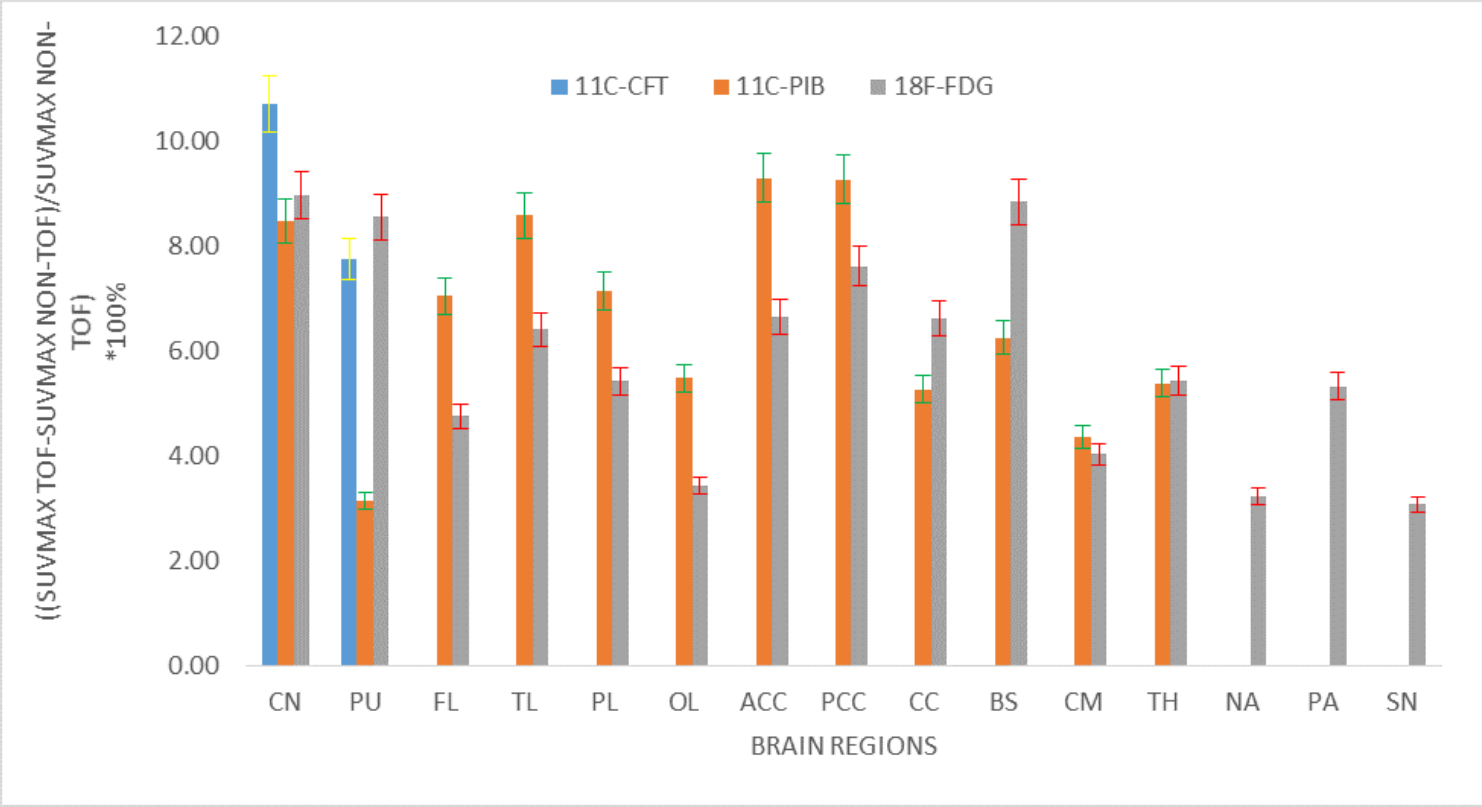

Figure 2

The % relative average difference of SUVmax in 11C-CFT (blue), 11C-PIB (red) and 18F-FDG (ash). CN: Caudate Nuclei; PU: Putamen; FL: Frontal Lobe; TL: Temporal Lobe; PL: Parietal Lobe; OL: Occipital Lobe; ACC: Anterior cingulate cortex; PCC: Posterior cingulate cortex; BS: Brainstem; CM: Cerebellar medulla; TH: Thalamus; NA: Nucleus Accumbens; PA: Pallidum; SN: Substantia Nigra.

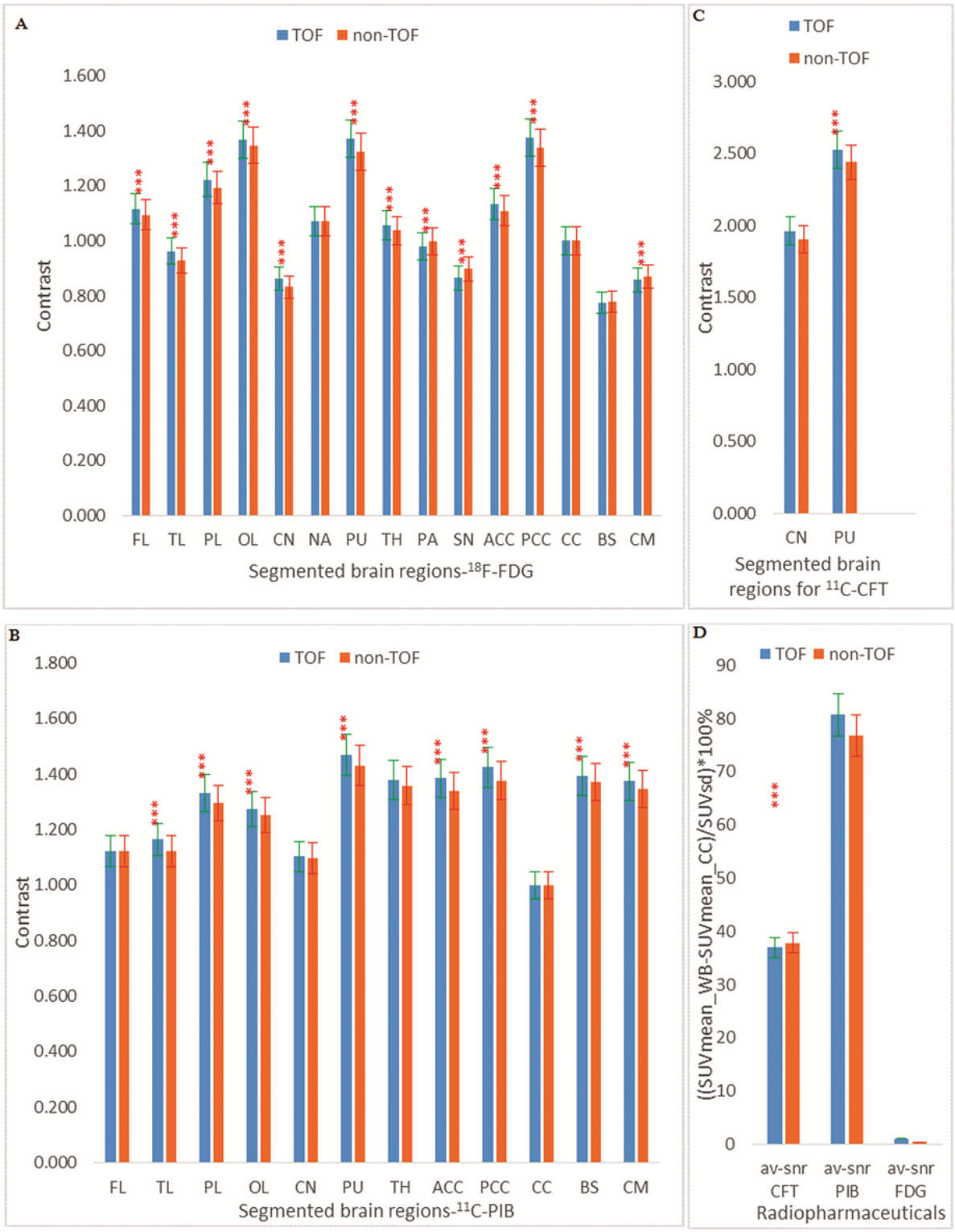

Figure 3

Illustration of VOI contrast and whole brain SNR% among 11C-PIB, 11C-CFT and 18F-FDG in the brain; ***: significantly difference ($p<0.05$) ;TOF: in blue color; non-TOF: in red color; A: VOI Contrast graph 18F-FDG; B: VOI Contrast graph 11C-PIB; C: VOI Contrast graph 11C-CFT D: %SNR in whole brain VOI (D). CN: Caudate Nuclei; PU: Putamen; FL: Frontal Lobe; TL: Temporal Lobe; PL: Parietal Lobe; OL: Occipital Lobe;

ACC: Anterior cingulate cortex; PCC: Posterior cingulate cortex; BS: Brainstem; CM: Cerebellar medulla; TH: Thalamus; NA: Nucleus Accumbens; PA: Pallidum; SN: Substantia Nigra.

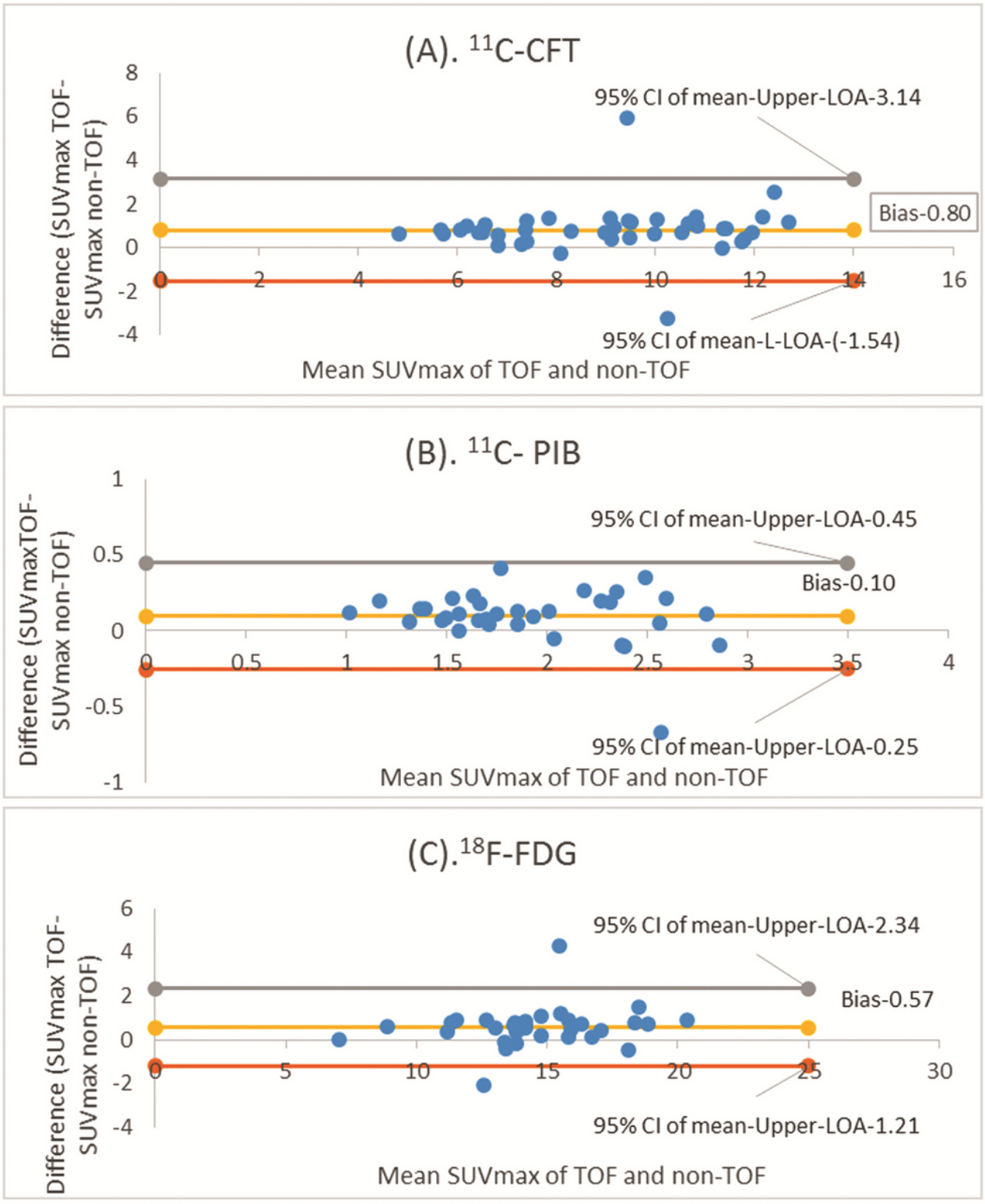

Figure 4

Bland-Altman plots 11C-CFT (A), 11C-PIB (B) and 18F-FDG(C); CI: Confidence interval; LOA: Line of agreement

Supplementary Files

This is a list of supplementary files associated with this preprint. Click to download.

- SupplementDataforsubmmision2.docx